Analysis of Nanoparticle Agglomeration in Aqueous Suspensions via Constant-Number Monte Carlo Simulation

ARTICLE *in* ENVIRONMENTAL SCIENCE & TECHNOLOGY · SEPTEMBER 2011

Impact Factor: 5.33 · DOI: 10.1021/es202134p · Source: PubMed

5 AUTHORS, INCLUDING:

Haoyang Haven Liu

10 PUBLICATIONS **115** CITATIONS

SEE PROFILE

Robert Rallo

Universitat Rovira i Virgili

87 PUBLICATIONS **1,232** CITATIONS

SEE PROFILE

Yoram Cohen

University of California, Los Angeles

262 PUBLICATIONS **5,943** CITATIONS

SEE PROFILE

Environmental Science & Technology

ARTICLE

pubs.acs.org/est

Analysis of Nanoparticle Agglomeration in Aqueous Suspensions via Constant-Number Monte Carlo Simulation

Haoyang Haven Liu,[†,‡] Sirikarn Surawanvijit,[†,‡] Robert Rallo,[†,§] Gerassimos Orkoulas,[‡] and Yoram Cohen*[,†,‡]

[†]Center for the Environmental Implications of Nanotechnology, California NanoSystems Institute, University of California, Los Angeles, Los Angeles, California 90095, United States

[‡]Chemical and Biomolecular Engineering Department, University of California, Los Angeles, Los Angeles, California 90095, United States

[§]Departament d'Enginyeria Informatica i Matematiques, Universitat Rovira i Virgili, Av. Paisos Catalans 26, 43007 Tarragona, Catalunya, Spain

Supporting Information

ABSTRACT: A constant-number direct simulation Monte Carlo (DSMC) model was developed for the analysis of nanoparticle (NP) agglomeration in aqueous suspensions. The modeling approach, based on the "particles in a box" simulation method, considered both particle agglomeration and gravitational settling. Particle−particle agglomeration probability was determined based on the classical Derjaguin−Landau−Verwey−Overbeek (DLVO) theory and considerations of the collision frequency as impacted by Brownian motion. Model predictions were in reasonable agreement with respect to the particle size distribution and average agglomerate size when compared with dynamic light scattering (DLS) measurements for aqueous TiO_2, CeO_2, and C_{60} nanoparticle suspensions over a wide range of pH (3−10) and ionic strength (0.01−156 mM). Simulations also demonstrated, in quantitative agreement with DLS measurements, that nanoparticle agglomerate size increased both with ionic strength and as the solution pH approached the isoelectric point (IEP). The present work suggests that the DSMC modeling approach, along with future use of an extended DLVO theory, has the potential for becoming a practical environmental analysis tool for predicting the agglomeration behavior of aqueous nanoparticle suspensions.

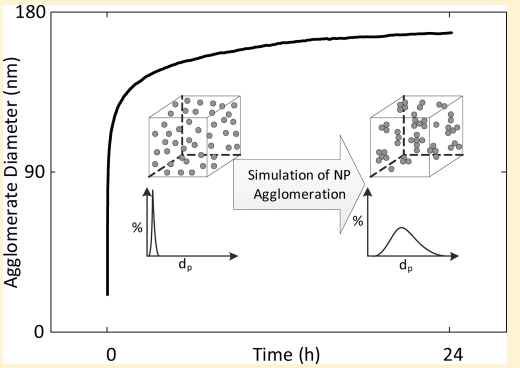

INTRODUCTION

Nanosized materials are increasingly being utilized in various modern industrial products and processes, primarily due to their unique nanoscale properties.[1−4] Engineered nanomaterials (eNMs) are estimated to be components of more than 1000 commercial products,[5] and thus there is an increased public concern regarding the potential adverse impacts of exposure to eNMs that may take place in the workplace, during product use and disposal, and in the environment.[4,6−11] The environmental transport and fate of eNMs[3,12] as well as their behavior at the bio−nano interface[3,10,13] are affected by their physicochemical properties[10] with the particle size being a major factor.[2,12] Fundamentally, mass diffusivity, sedimentation velocity, deposition velocity, and attachment efficiency of nanoparticles onto solid and biological surfaces are significantly influenced by their size.[14−17] As has been shown in numerous studies, nanoparticles in aqueous suspensions, which are the focus of the present study, generally do not exist as stable suspensions of primary nanoparticles.[12,18−24] This is particularly the case under environmental conditions where the ionic strength of natural water sources is sufficiently high and where adsorption of hydrophobic organics onto the nanoparticles[25,26] can both promote rapid nanoparticle agglomeration.[18−20,23]

In recent years, efforts to quantify the agglomeration state of eNMs have intensified.[12] However, comprehensive experimental mapping of eNMs agglomeration for the large number of present and anticipated emerging nanoparticles, over wide ranges of possible environmental water chemistries and nanoparticle properties, is a daunting and possibly impractical task. Thus, there has been a growing interest to explore various approaches[18,27−29] to better understand and generalize the agglomeration behavior of nanoparticles in aqueous suspensions. The majority of studies on the environmental or toxic impact of nanoparticles have focused on qualitative interpretation of observed agglomeration behavior of nanoparticles via the classical DLVO theory.[18,19,21,22] Yet, there are factors (e.g., steric, geometric, hydrodynamic, hydration, magnetic) that can impact nanoparticle agglomeration that are not considered by the classical DLVO theory. Accordingly, extended versions of the DLVO theory have been proposed.[30−34] It has been generally accepted, however, that classical DLVO theory can provide a reasonable starting point for describing nanoparticle agglomeration in aquatic media under a wider range of environmental conditions[12,15,18,28] and even for surface coated nanoparticles.[28]

Received: June 22, 2011
Accepted: September 14, 2011
Revised: August 29, 2011
Published: September 14, 2011

Quantitative simulation methods to describe agglomeration of nanoparticles can be implemented while accounting for particle−particle interactions.[15,35−38] Indeed, molecular dynamics (MD) and Brownian dynamics (BD) simulations have been used to study details of nanoparticle agglomeration kinetics and agglomerate morphology.[35−37] BD simulations of nanoparticle agglomeration in aqueous suspensions have demonstrated that the DLVO theory can provide a reasonable description of nanoparticle agglomeration.[39] It has been shown that that BD type simulations can track the temporal change in nanoparticle suspension concentration due to sedimentation.[40] Also recent comparison of the MD and BD methods[37] revealed that nanoparticle clusters with higher fractal dimensions were predicted with the MD approach. While MD and BD methods provide detailed information regarding particle agglomeration/disagglomeration via tracking of individual particles, they do so at the expense of significant computational resources. Thus, these methods place a limit on the practical number of particles that can be effectively modeled.[36,39] Another popular approach is the class of direct simulation Monte Carlo (DSMC) methods which treats the simulation domain as a statistical particle ensemble where each event has a probability of occurrence quantified via frequency functions calculated based on particle−particle interaction energies.[36,41,42] The DSMC simulation approach[36,38,41−46] is a convenient method for describing particle agglomeration based on solving the population balance equations (PBEs) as described by the classical Smoluchowski coagulation equation[47,48] or its extension to include disagglomeration[43] nucleation and surface growth.[36]

DSMC methods can be conveniently applied with moderate computational resources, in conjunction with the DLVO approach (or its extension) to quantitatively describe nanoparticle agglomeration in aqueous suspensions. In addition, most laboratory experiments dealing with the fate and transport[20,21,24,27,44] or toxicity[13,49,50] of nanoparticles in aqueous suspensions are typically conducted over extended periods of time (hours to days). Environmental time scales of interest are also of similar or longer magnitude. Therefore, model simulations need to consider the evolution of the particle size distribution (in aqueous suspension) to its steady-state (or stable) condition given the combined effects of agglomeration and sedimentation. Experimental studies have documented the sedimentation of agglomerated nanoparticles, based on UV−vis spectrometry[20,21,51,52] and visual observations[53,54] for measurement time scales on the order of hours[20,21,52] to days.[51,53,54] For example, studies with aqueous nanoparticle suspensions (∼10−200 mg L^{-1}) have demonstrated significant concentration decrease (up to ∼90% in some cases) for TiO_2[21,31] (21 nm) and iron-based[52] (50 nm) nanoparticles over a period of up to ∼6 h.

In the present study, nanoparticle agglomeration is investigated within the context of the DLVO theory based on a computational constant-number DSMC approach[41,42] of "particles in a box" considering Brownian motion and agglomerate sedimentation. In this approach, evolution of the particle size distribution is tracked to its steady state condition with model validation based on present experimental and literature reported dynamic light scattering (DLS) measurements of agglomerates sizes for TiO_2, CeO_2, and C_{60} nanoparticles in aqueous suspensions. A series of parametric simulations were also carried out in order to illustrate the influence of various model parameters (e.g., primary nanoparticle diameter, pH) on nanoparticle agglomeration behavior and thus suggest the potential use of the DSMC modeling approach and its potential extension (e.g., modified DLVO), as a useful tool for the study of nanoparticle agglomeration in aqueous suspensions.

MATERIALS AND METHODS

Evaluation of Nanoparticle Agglomeration. The agglomerate size of nanoparticles in aqueous suspensions was evaluated via a constant-number DSMC approach[42] making use of the classical DLVO theory[48,55] and accounting for agglomerate sedimentation. The modeling approach focused on enabling comparison of predicted and measured (via DLS) nanoparticle agglomerate sizes (in aqueous suspensions) over a period (24 h) typical in high throughput nanoparticle toxicity screening studies.[21,49]

Experimental Section. The agglomeration state of TiO_2 (Evonik Industries, Parsippany, NJ) and CeO_2 (Meliorum Technologies, Rochester, NY) nanoparticles (21 and 15 nm primary diameter, respectively; Supporting Information (SI), Figure S9) was quantified in aqueous suspensions over a pH range of 3−10 and ionic strength (IS) of 10^{-2}−1 mM. Aqueous suspensions of the commercial nanoparticles were prepared using 18 MΩ cm ultrapure D.I. water with pH adjustment using HCl, NaOH and $NaHCO_3$ and NaCl for ionic strength adjustment (ACS grade, Fisher Scientific, Waltham, MA).

Nanoparticle stock suspensions were first prepared at a concentration of 1000 mg L^{-1} by adding (over a ∼5 s period) 10 mg of nanoparticles to a stirred 10 mL volume of water (in a 40 mL vial) previously adjusted to pH of 3 or 10; stirring was accomplished using a Teflon coated 15.8 mm (L) x 8 mm (D) magnetic stir bar and stirrer (Magnestir S8290, Scientific Products, McGaw Park, IL). The resulting suspension was immediately sonicated for 30 min at 23 ± 0.5 °C in a temperature controlled sonication bath (Bransonic 2510, Branson, Danbury, CT, 0.75 gallon, 130 W @ 40 Hz). The sonication bath temperature was maintained (±0.5 °C) by circulating water through a copper coil tube (0.635 cm inside diameter), submerged in the sonication bath, from a constant temperature water circulator (NESLAB RTE-111, Thermo Scientific, Waltham, MA). Maintaining a constant temperature in the sonication bath was essential since, in the absence of temperature control, significant temperature rise was observed (up to ∼20 °C over a 30 min period) as a consequence of the sonication process. It is noted that a sonication period longer than about 30 min did not improve nanoparticle dispersion. After sonication, 0.4 mL of the suspension was withdrawn and added to 19.6 mL of the same pH adjusted water in a 40 mL glass vial (resulting in 20 mg L^{-1} suspension) with additional 5 min sonication also at 23 °C. Nanoparticle suspensions at pH 8 were prepared by a similar procedure, but with 0.4 mL of a 1000 mg L^{-1} pH 10 stock suspension added to a 19.6 mL water at pH 8 and 2.4×10^{-4} mM $NaHCO_3$. Immediately after 5 min sonication of the 20 mg L^{-1} (20 mL) suspension, 3 mL sample was transferred to a 4.5 mL cuvette for DLS analysis of the particle size distribution.

Particle size distribution (PSD) measurements for the different nanoparticle suspensions were obtained via DLS measurements (ZetaSizer Nano S90, Malvern Instruments, Worcestershire, U.K.) over a 24 h period. This DLS instrument utilizes a horizontal entry laser beam of ∼40 μm in diameter, and detection angle of 90° with measurement reliability down to ∼0.25 mg L^{-1}.[56] In the present study, the nanoparticle concentration decreased from its initial value of 20 mg L^{-1} to 1−17 mg L^{-1} (depending on the pH and ionic strength) and thus all DLS measurements were at concentrations above the minimum detection limit. The mass concentrations

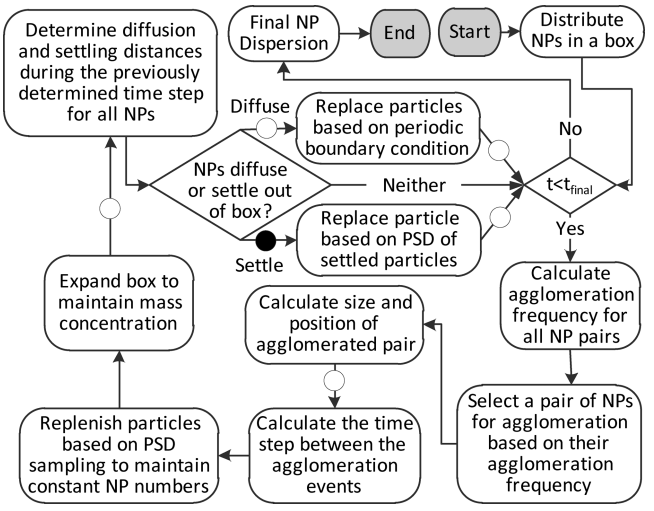

Figure 1. Flow diagram of the Monte Carlo particles in a box simulation. The open and filled circles indicate the points in the algorithm at which the particle size distributions are determined for the particles in suspension and the settled particles, respectively.

of the nanoparticles in the stock solutions and in samples used for DLS measurements were determined via elemental analysis of the suspension, by inductively coupled plasma mass spectrometry (ICP-MS) following a previously published protocol.[57] Finally, zeta potential for the nanoparticles was measured (Brookhaven ZetaPAL, Brookhaven Instruments, Holtsville, NY) for the above nanoparticle suspensions at ionic strength of 0.1 mM.

Simulation Algorithm. A constant-number DSMC model of particles in a box[42] was developed to describe nanoparticle agglomeration in suspensions while accounting for agglomerate sedimentation. The accuracy of the DSMC simulations varies with the number of particles, N, in the simulation domain (i.e., box) with the error $\propto 1/\sqrt{N}$.[45] Therefore, the number of particles was kept constant[42] and the nanoparticle mass concentration was preserved through simulation box expansion.[41] The simulation algorithm is described in Figure 1 with details of the working equations provided in Table S1 (Supporting Information (SI)).

The simulation approach (Figure 1) consists of initially distributing N nanoparticles (NP) in a simulation box (SI, Figure S1) of dimensions that are consistent with the desired nanoparticle mass concentration. The agglomeration frequencies for each of the N^2 pairs of particles are calculated following the approach of the Smoluchowski coagulation equation.[55] Subsequently, a pair of particles is selected for agglomeration based on a probability density function constructed from the agglomeration frequencies (SI, Figure S2), and the size and position are then computed for the agglomerated particle pair. Only pairwise particle−particle interactions are considered[48,55] and the agglomeration events assumed to be irreversible.[18,25] The time step for each consecutive agglomeration event is determined based on the inverse of agglomeration frequency (eq 7).[38,41,42] Each agglomeration event reduces the total number of particles (i.e., freely suspended primary particles and agglomerates) by one. Therefore, following each agglomeration event, a particle is added to the box in order to preserve the total number of particles in the box. The added particle is selected by sampling from the particle size distribution of the particles in the simulation box. In order to preserve the mass concentration of nanoparticles, the simulation box is expanded to accommodate the added mass contributed by the above step of particle replenishment (SI, Figure S1). Particles can move out of the box due to gravitational sedimentation. A particle that has settled out of the box is replaced by a particle selected from the size distribution of the particles that have settled. For particles that have traveled out of the box (top or sides) by Brownian motion, periodic boundary conditions[15] are invoked to replace the particles (i.e., the same removed particle is placed back into the box).

Model Equations. The simulation is initialized by first distributing N nanoparticles in a simulation box of volume V [m^3] satisfying the initial particle mass concentration, C_o [mg L^{-1}]:

$$V = \frac{\rho}{C} \cdot \sum_{i=1}^{N} \left(\frac{4}{3} \pi \cdot r_i^3 \right) \tag{1}$$

where ρ [g m^{-3}] is the nanoparticle density, C is the mass concentration [mg L^{-1}], and r_i [m] is the radius of particle i. The initial nanoparticles in the simulation box (SI, Figure S1) are positioned at locations $(x_i y_i z_i) = (V)^{1/3} \cdot [P_x P_y P_z]$, where the random numbers P_x, P_y, and P_z are uniformly distributed in [0,1], while disallowing two particles to occupy the same space.

The agglomeration frequency $\hat{N}_{ij}$, [no. of agglomeration events per m^3 s] between two particles i and j is determined based on the Smoluchowski coagulation theory where[47,55,58]

$$\hat{N}_{ij} = k_{ij} \cdot n_i \cdot n_j \tag{2}$$

where n_i and n_j are the number concentrations of particles i and j, respectively. The agglomeration frequency function, k_{ij}, is expressed as:

$$k_{ij} = \frac{\beta_{ij}}{W_{ij}} \tag{3}$$

in which β_{ij} is the collision frequency function which arises due to Brownian motion[42,48] given by

$$\beta_{ij} = \frac{2kT}{3\mu} (r_i + r_j) \left(\frac{1}{r_i} + \frac{1}{r_j} \right) \tag{4}$$

where r_i and r_j are the effective radii [m] (eq 6) of particles i and j, respectively, k is Boltzmann's constant [$k = 1.38 \times 10^{-23}$ J K^{-1}], T is temperature [K], and μ is the viscosity of the medium [Pa s]. The stability ratio, W_{ij} [dimensionless], is the inverse of the fraction of successful collisions for particle pair i,j, given as[48,55]

$$W_{ij} = \frac{\text{no. of collisions}}{\text{no. of collisions that result in agglomeration}} = 2 \cdot \int_2^{\infty} \frac{\exp\left[\frac{\Phi_{T,ij}}{kT}\right]}{s^2} ds \tag{5}$$

in which $s = 2R/(r_i + r_j)$, where R is the distance between the center of the particles [m], and $\Phi_{T,ij}$ is the total interaction energy [J] between particle pair i,j. There are various approaches to quantifying $\Phi_{T,ij}$;[31,55] however, in the present work the classical DLVO theory[48,55,58] (SI, Table S1) was adopted as a first order analysis, without a loss of generality of the simulation approach, given its success in describing surface interactions in colloidal systems.[48,55,58] Recent studies have also suggested that the DLVO approach is a reasonable basis for quantifying the agglomeration of nanoparticles.[12,15,18] According to the classical DLVO theory, the total interaction energy for a particle pair is the

sum of the van der Waals attraction energy (as a function of the Hamaker constant A_H [J], particle sizes r_i and r_j [m], and separation distance between the particle pair R [m])[48,58] and the electrical double layer repulsion energy (being a function of the surface zeta potential of nanoparticles in solution ζ [V], solution ionic strength IS [M], r_i, r_j, and R) as summarized in Table S1 (SI). Other model parameters include the primary nanoparticle diameter d_p [m], initial nanoparticle concentration C_o [mg L^{-1}], agglomerate fractal dimension d_f [dimensionless],[47] and primary particle density ρ [g m^{-3}].

Once the agglomeration frequency function is determined (eq 3) for all particle pairs, a pair of nanoparticles (i,j) is selected to agglomerate following the sampling approach proposed by Kruis et al.,[45] where the probability for the selected pair is taken to be proportional to the relative magnitude of its agglomeration frequency function (SI, Figure S2). In this approach, the k_{ij} values are added sequentially for the list of all particle pairs until the k_{ij} sum exceeds the value of a sampled random number R in $[0, \sum_{i=1}^{N}\sum_{j=1}^{N} k_{ij}]$. When the above criterion is satisfied, the particle pair (i,j) corresponding to the last added k_{ij} is selected for agglomeration. The mass of this newly formed agglomerate, m_k, is the linear sum of the agglomerated particle pair, that is, $m_k = m_i + m_j$. The effective diameter of this agglomerate, d_e, is calculated as:[59]

$$d_e = d_p \cdot n_p^{1/d_f} \tag{6}$$

where n_p is the number of primary particles in the agglomerate, and d_f is the fractal dimension for the specific agglomeration regime.[47] In order to maintain the total particle count in the simulation box, the lost particle (due to agglomeration) is replenished by sampling from the existing particle size distribution. The simulation box is then expanded to a new volume (eq 1) in order to maintain the mass concentration. The box is expanded horizontally (in the x,y plane; SI, Figure S1) in order to maintain consistency with experimental DLS measurements in which the thickness of the laser beam is fixed. Following box expansion (Figure 1), the time step $[s]$ to the next agglomeration event is estimated based on the inverse of the average agglomeration frequency function $\langle k_{ij} \rangle$ over all N^2 particle pairs:[42]

$$\Delta t = \frac{2}{C \cdot N \cdot \langle k_{ij} \rangle} \tag{7}$$

Diffusion and settling distances due to Brownian diffusion and Stokes' sedimentation, respectively, are subsequently determined for the above time step (eq 7) for all particles in the box. The vertical distance traveled by a particle i is estimated as

$$\Delta z_i = z_{S,i} + z_{B,i} \tag{8}$$

where $\Delta z < 0$ represents net downward movement. The gravitational settling distance for particle i is given as $z_{S,i} = -v_{S,i} \cdot \Delta t$, where $v_{S,i}$ is its Stokes' settling velocity given by[14]

$$v_{S,i} = \frac{2(\rho_p - \rho_f) \cdot (1 - \phi_i) \cdot g \cdot r_i^2}{9 \cdot \mu} \tag{9}$$

in which ρ_p is the particle density (g L^{-1}), ρ_f is the fluid density, g is the gravitational constant [m^3 kg^{-1} s^{-2}] and ϕ is the particle agglomerate porosity (i.e., $\phi = 1 - (r_m/r_e)^3$, where r_m is the mass equivalent radius of the particle ($r_m = ((3m_i)/(4\rho\pi))^{1/3}$, [m]), and r_e is its effective radius (eq 6). The Brownian diffusion distance, $z_{B,i}$ (positive or negative for upward or downward movement, respectively) is estimated assuming that the distance traveled vertically is determined based on a random number sampled from a normal distribution with $\mu = 0$ and $s = (2 \cdot D_i \cdot \Delta t)^{1/2}$ [47,55] such that $z_{B,i} \sim \mathbb{N}(0, 2 \cdot D_i \cdot \Delta t)$, in which D_i is the Brownian diffusivity [m^2 s^{-1}] determined from[47,55] $D_i = (kT)/(6\pi\mu r_i)$. Following the above approach, particles for which $z_i + \Delta z_i \leq 0$ (where z_i is the particle vertical position at time t_i) are considered to have settled out of the box, thereby decreasing the number of particles in the box. This necessitates the introduction of new particles into the box in order to preserve the total particle count. The size of each replenishing particle is determined by sampling from the size distribution of the last N particles that have settled, given the expectation that particles can enter the box via its top face via sedimentation. The vertical positioning of each replenishing particle in the simulation box is assigned as $z_i = L_z + P_z \cdot \Delta z_i$, where L_z is the box height, and P_z is a uniformly distributed random number in $[0,1]$. Δz_i is the vertical distance that would be traveled due to the combined effect of sedimentation and Brownian motion, calculated as described above, for the same agglomeration time step (eq 7). The above sampling is repeated until the condition, $0 < z_i \leq L_z$, for placing a particle inside the box is met and the mass concentration in the box is recalculated. Finally, it is noted that particles can diffuse out of the vertical sides of the simulation box due to Brownian motion. However, in this case, one can invoke a periodic boundary condition specifying that a particle that diffuses out of a given vertical face would be reintroduced from the opposite face. A similar reasoning is applied to particles that diffuse out of the box through the top (horizontal) face.

Simulations. Simulations were performed for TiO_2 and CeO_2 nanoparticles of 21 and 15 nm primary particle diameters, respectively, at initial concentration of 20 mg L^{-1}, matching the 24 h period of DLS measurements (SI, Table S2). Simulation conditions also matched the pH range of 3−10, and ionic strength of 0.02−0.4 mM at 23 °C for the present DLS measurements. For comparison with reported literature data for TiO_2 nanoparticle suspensions, additional simulations were also carried out for an initial concentration range of 40 − 50 mg L^{-1}, pH of 3−10.4, and IS of 0.01 − 12.5 mM.[21,22,24] Simulations were also carried for aqueous C_{60} nanoparticle suspensions (primary size of 80 and 168 nm), pH 5.5, 7 and ionic strength of 10−156 mM. The basic fundamental model parameters included: particle primary size, zeta potential, Hamaker constant, solution ionic strength and temperature. The first three parameters were obtained from either independent measurements or from literature reported data (See SI, Table S2), while the latter two were the conditions as specified in the particular experiments. Therefore, all model simulations that are compared with experimental data are a priori predictions. Simulations were carried out with a number of particles in the box ranging up to 10 000. Different numbers of repeated simulations (for the same particle number) were carried out in order to evaluate the optimally reasonable number of particles needed to achieve convergence of the simulation results. Simulations were carried out on a cluster of 20 Intel Xeon Quad-Core processors at 2.2−3.0 GHz with 176 GB of total RAM. Simulation CPU times on this cluster ranged from as short as 100 s to as along as 15 days for 500 and 10 000 simulated nanoparticles, respectively.

RESULTS AND DISCUSSION

Convergence of Simulations. Simulations of nanoparticle agglomeration were first carried out to determine the number of particles necessary to achieve a convergent solution. A series of

simulations with 500−10 000 nanoparticles in the simulation box indicated, consistent with the existing DSMC literature, that the use of 5000 particles (e.g., Figure 2 and SI, Figure S3) was sufficient for reaching accurate simulation results.[36,38] However, given that the simulations were seeded with random numbers (Figure 1; SI, Figure S2), there were statistically measurable variations in the results for repeated simulations (e.g., SI, Figure S4). It is found that above five replicate simulations and with 5000 (or more) particles in the simulation box, the change in the predicted average agglomerate size was less than 0.1% (e.g., SI, Figure S4b) and the standard deviation of the predicted average agglomerate size over 10 replicate simulations was typically below 1% (Figure 2; SI, Figures S3). Accordingly, all results in the present work are presented as the average over 10 simulation replicates for 5000 particles in the simulation box.

Nanoparticle Agglomeration. As nanoparticles agglomerate in aqueous suspensions, gravitational sedimentation can take place thereby altering the size distribution of the particles remaining in suspension. For example, nanoparticle agglomerates of size 100 and 250 nm can sediment a distance equivalent to a typical width of a DLS laser beam (∼0.04 mm) in a period of 7 and 1 h, respectively (SI, Figure S5). Thus, if nanoparticle agglomerates reach the above size range or greater, settling due to gravity has to be considered, especially for applications and studies of extended duration. Of particular interest in the present study are predictions of agglomerate sizes as determined by DLS measurements in the presence of particle settling. The occurrence of sedimentation can be inferred from a decrease in the photon count rate in DLS measurements. This is illustrated, for example, in Figure S6 (SI) revealing ∼18% and ∼30% photon count rate decrease in DLS measurements over a 24 h period for TiO_2 (pH 8 and 10, IS = 0.37 mM) and CeO_2 (pH 8, IS = 0.37 mM) nanoparticles, respectively. The simulations revealed a rapid rate of agglomeration with an agglomerate size that increases with time when sedimentation is not considered in the model. However, upon inclusion of sedimentation a "stable" (i.e., time independent) agglomerate size is reached (in suspension) after several hours. This behavior is illustrated in Figure 3 for CeO_2 and TiO_2 nanoparticles of 15 and 21 nm primary particle diameters, respectively, at pH 8 at low ionic strength of 0.065 mM. As a result of sedimentation, the mass concentration of the TiO_2 and CeO_2 nanoparticles in suspension decreased by 10−50% for the present range of simulation conditions (SI, Table S2) as was verified via ICP measurements; however the average particle size in suspension remained essentially at steady state (after ∼15 h, Figure 3). Such behavior is reached once the rate of sedimentation is balanced by the rate of nanoparticle agglomeration. The predicted average agglomerate size is in remarkable agreement with the present DLS measurements (Figure 3) with a prediction absolute error of 1% and 0.4% for TiO_2 and CeO_2 nanoparticles for the solution conditions indicated in Figure 3. However, it is noted that sonication of the suspensions, prepared from commercial nanoparticle powders, could only breakup the nanoparticle agglomerates to their "stable" suspension particle size. Therefore, the region of agglomerate evolution could not be traced via DLS and only the stable nanoparticle agglomerate size could be monitored (Figure 3).

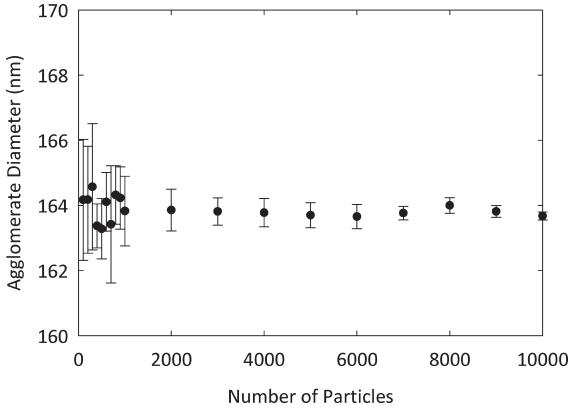

Figure 2. Mean agglomerate diameter based on the average of 10 simulations as a function of the number of particles in the simulation box. The vertical bars represent one standard deviation of the mean particle size over 10 simulation replicates. Simulation conditions: $\zeta = -40$ mV, IS = 0.1 mM, $d_p = 21$ nm, $A_H = 42$ zJ.

Comparison of MC model predictions of TiO_2 nanoparticle agglomerate size with the present series of DLS measurements and published literature data[21,22,24,60,61] along with comparisons of predictions with literature data for C_{60} nanoparticles are provided in Figure 4 and Table S2 (SI). Only literature data for agglomerate sizes below 1 μm were considered as this size approaches the limitations of DLS measurements[56] as well as the DLVO theory.[55] Reasonable agreement of predictions with DLS data (present and literature data) were obtained with an absolute error in the range of 0.6−25.3% and ∼10.8% average absolute

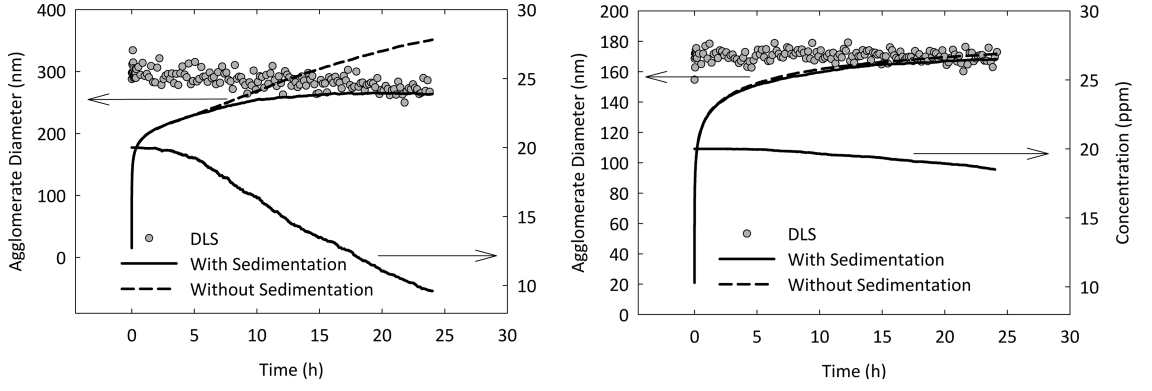

Figure 3. Evolution of CeO_2 (left) and TiO_2 (right) agglomerate diameter based on simulation with and without sedimentation, based on average of 10 simulation instances with 5000 particles in the simulation box. Simulation conditions: pH 8, $\zeta_{CeO_2} = -24.5$ mV, $\zeta_{Tio_2} = -29$ mV, IS = 0.065 mM, $A_{H,CeO_2} = 21$ zJ, $A_{H,TiO_2} = 42$ zJ.

error for the 26 measurements depicted in Figure 4 (also SI, Table S2). Notwithstanding the success of the constant-number DSMC model predictions (Figures 3 and 4; SI, Table S1) of nanoparticle agglomeration, broader assessment of the suitability of the present simulation approach for predicting short-time agglomeration kinetics would necessitate DLS measurements with aqueous suspensions in which the nanoparticles are initially near their primary diameter.

Dependence of Nanoparticle Agglomeration on Model Parameters (d_p, ζ, IS, A_H). According to the DLVO theory[48,55] nanoparticle agglomeration depends primarily on the nanoparticle primary diameter (d_p), Hamaker constant (A_H), ionic strength (IS), and surface electrical potential (estimated from the zeta potential, ζ). The zeta potential varies with solution pH and there is a pH at which the isoelectric point (IEP) is reached where the net surface charge is zero (i.e., ζ = 0 mV). Particle agglomeration is expected to be most significant near the IEP as the electrical double layer diminishes and the attractive energy due to van der Waals forces becomes dominant. As the solution pH deviates away from the IEP, the electrical double layer thickness increases as does the surface charge (either positive or negative; Figure 5a) and thus greater particle repulsion and smaller agglomerates are expected. The above behavior is demonstrated in Figure 5a for simulations of TiO_2 nanoparticle agglomerates revealing agreement with measured DLS data within an absolute average error of 2.8%. The predictions are consistent with experimental observations of the maximum agglomerate particle size (400 nm) at the IEP and decreasing size away from the IEP (by about a factor of 3 for the measurements at the lowest and highest pH levels). As shown in Figure 5b, nanoparticle agglomeration can also increase with increased ionic strength due to suppression of the electrical double layer. The typical reported dependence of particle agglomeration on ionic strength[22] is illustrated in the simulation results shown in Figure 5b for TiO_2 nanoparticles (d_p = 21 nm) at ζ = 20 mV and 40 mV. In this example, the critical coagulation concentrations at the above two conditions are estimated at ~0.08 mM and ~2.89 mM at which the agglomerate size is ~805 nm and ~563 nm, respectively. Although the predicted rise in agglomerate size at high ionic strength portrays the expected trend, the deviation of the calculated average agglomerate size from the mean is noteworthy. Considerably more than 10 simulation instances with N > 5000 would have been necessary (at the expense of considerable CPU time of ~4 weeks) to achieve an accurate stationary solution, since the size fluctuation is large at high IS due to a significant degree of settling. According to the DLVO theory, agglomerate sizes would also increase with increasing magnitude of the Hamaker constant, as this would imply increasing van der Waals attraction energy (SI, Table S1, eq S1). For the above TiO_2 example, the simulations reveal a linear dependence of agglomerate nanoparticle size on the Hamaker constant (A_H) demonstrating an agglomerate size increase from 110 nm to 550 nm with A_H increase from 10 zJ to 90 zJ (SI, Figure S7), corresponding to the range of literature reported A_H values for the anatase[62,63] and rutile[63,64] forms of TiO_2.

The simulations revealed that the agglomerate size of nanoparticles in aqueous suspension increases with decreasing primary particle diameter (Figure 6). This result should not be surprising since van der Waals interactions increase with decreasing particle size (SI, eq S1), the collision frequency is more pronounced with smaller particles (eq 4) and electrostatic repulsion increases with increased particle size (SI, eqs S2 and S3). As a result, smaller primary nanoparticles will form larger agglomerates. It is noted, however, that DLS measurements are only indicative of the size of particles remaining in suspensions and do not provide a measure of the true distribution of all

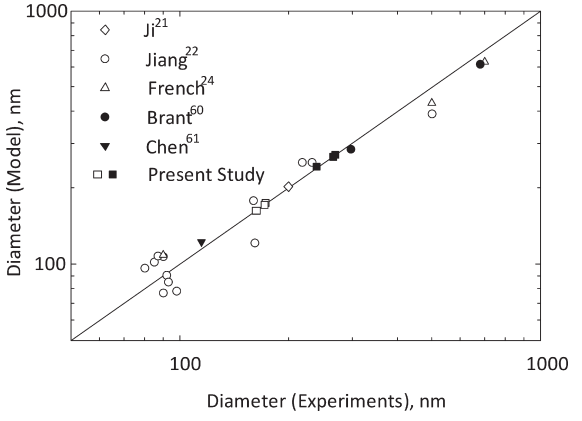

Figure 4. Comparison between simulation and experimental results for average agglomerate diameter for TiO_2,[21,22,24] CeO_2, and C_{60}[60,61] nanoparticles. For TiO_2, d_{p,TiO_2} = 5 (Δ), 15 (O), and 21 (◇, □) nm, for CeO_2, d_{p,CeO_2} = 15 (■) nm, and for C_{60}, $d_{p,C_{60}}$ = 80 (▼) nm, 168 (●) nm. IS = 0.01−156 mM, pH 3−10.4, ζ = −45−42 mV.

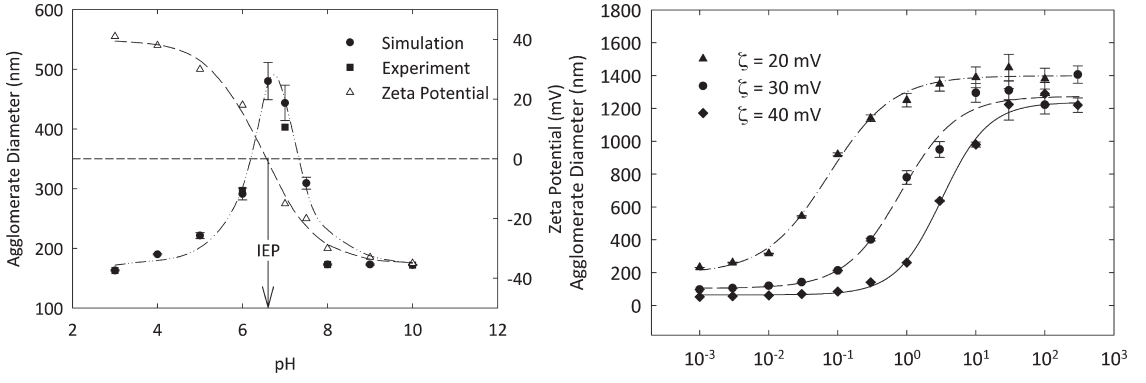

Figure 5. Average agglomerate diameter of nanoparticle aggregates after 24 h as a function of (left) pH levels (at IS = 0.037 mM) and (right) ionic strength. Simulation conditions: A_H = 42 zJ, d_p = 21 nm, C_o = 20 mg L^{-1}, temperature = 23 °C. Note: the vertical bars represent one standard deviation over 10 simulation replicates.

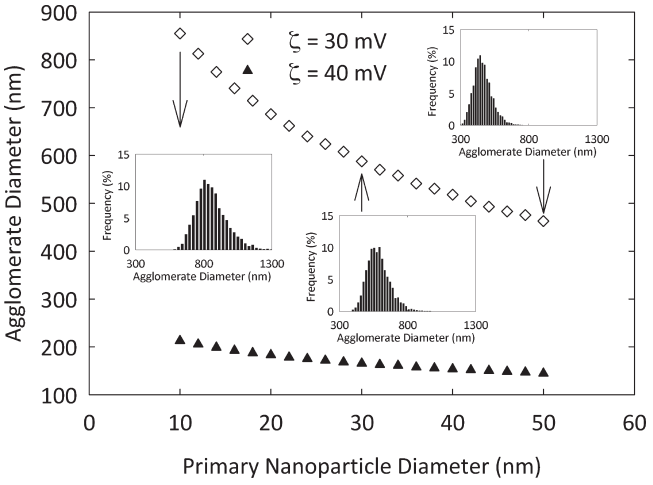

Figure 6. Dependence of average agglomerate diameter on the primary nanoparticle diameter. Simulation condition: IS = 0.5 mM, C_o = 20 mg L^{-1}, T = 23 °C.

agglomerates that may have formed. Accordingly one would expect that, as a result of agglomeration and sedimentation, the nanoparticle size distribution in suspension (as determined by DLS) will reveal an increasing tail of smaller size agglomerates with increasing primary particle diameter (Figure 6; SI, Figure S8). The above behavior should not be taken as a universal representation of nanoparticle agglomeration as one must be cautious with the limitation of the DLVO theory to nanoparticles with $\kappa r \ll 1$ (e.g., corresponding to $r_i \ll 10$ nm at IS = 1 mM; note that κ is the inverse Debye length, SI, Table S1). Moreover, it is also noted that the present application of the DLVO theory, as well as the simple application of gravitational settling, does not consider the impact of the details of agglomerate geometry and morphology. Nonetheless, the present analysis suggests that interpretation of nanoparticle behavior in environmental aquatic media and potential toxic outcomes due to exposure to nanoparticles must carefully consider not only the particle size distribution but also the experimental protocols used to determine such size distributions.

In summary, the present constant-number DSMC approach of simulating nanoparticle agglomeration in aqueous suspensions demonstrated that classical DLVO theory can provide reasonably accurate predictions of the average nanoparticle agglomerate size as well as the particle size distribution over a wide range of solution pH (3−10) and ionic strength (0.01−156 mM; SI, Table S2). Extension of the present approach using the extended DLVO theory is presently underway in order to explore a wide range of nanoparticle types aqueous solution chemistries of environmental interest.

■ ASSOCIATED CONTENT

Supporting Information. Additional information is included in the supporting information regarding figures of the box expansion approach, particle pair selection method, added figures of experimental and simulation results, calculation of sedimentation distances, TEM images of nanoparticles, list of DLVO working equations, and table of experimental and simulation conditions. This material is available free of charge via the Internet at http://pubs.acs.org/.

■ AUTHOR INFORMATION

Corresponding Author
*E-mail: yoram@ucla.edu.

■ ACKNOWLEDGMENT

This work was supported, in part, by the National Science Foundation and the Environmental Protection Agency under Cooperative Agreement Number DBI 0830117, the UCLA Water Technology Research Center and the California Department of Water Resources. Any opinions, findings, conclusions or recommendations expressed herein are those of the author(s) and do not necessarily reflect the views of the National Science Foundation or the Environmental Protection Agency. This work has not been subjected to an EPA peer and policy review. We also thank Zhaoxia Ji for assistance in obtaining the TEM images.

■ REFERENCES

(1) Guo, Z.; Tan, L. *Fundamentals and Applications of Nanomaterials*, 1st ed.; Artech House Publishers: Norwood, MA, 2009.

(2) Klaine, S. J.; Alvarez, P. J. J.; Batley, G. E.; Fernandes, T. F.; Handy, R. D.; Lyon, D. Y.; Mahendra, S.; McLaughlin, M. J.; Lead, J. R. Nanomaterials in the environment: Behavior, fate, bioavailability, and effects. *Environ. Toxicol. Chem.* **2008**, *27* (9), 1825–1851.

(3) Handy, R. D.; Owen, R.; Valsami-Jones, E. The ecotoxicology of nanoparticles and nanomaterials: Current status, knowledge gaps, challenges, and future needs. *Ecotoxicology* **2008**, *17* (5), 315–325.

(4) Wiesner, M. R.; Lowry, G. V.; Alvarez, P.; Dionysiou, D.; Biswas, P. Assessing the risks of manufactured nanomaterials. *Environ. Sci. Technol.* **2006**, *40* (14), 4336–4345.

(5) The Project on Emerging Nanotechnologies: Consumer Products Inventory (Woodrow Wilson International Center). http://www.nanotechproject.org/inventories/consumer/ (accessed 8/29/2011).

(6) Farré, M.; Gajda-Schrantz, K.; Kantiani, L.; Barceló, D. Ecotoxicity and analysis of nanomaterials in the aquatic environment. *Anal. Bioanal. Chem.* **2009**, *393* (1), 81–95.

(7) Barnard, A. S. Computational strategies for predicting the potential risks associated with nanotechnology. *Nanoscale* **2009**, *1* (1), 89–95.

(8) Stone, V.; Nowack, B.; Baun, A.; van den Brink, N.; von der Kammer, F.; Dusinska, M.; Handy, R.; Hankin, S.; Hassellöv, M.; Joner, E.; Fernandes, T. F. Nanomaterials for environmental studies: Classification, reference material issues, and strategies for physico-chemical characterisation. *Sci. Total Environ.* **2010**, *408* (7), 1745–1754.

(9) Kahru, A.; Dubourguier, H.-C. From ecotoxicology to nanoecotoxicology. *Toxicology* **2010**, *269* (2−3), 105–119.

(10) Biswas, P.; Wu, C. Y. Critical Review: Nanoparticles and the environment. *J. Air Waste Manage. Assoc.* **2005**, *55* (6), 708–746.

(11) Colvin, V. L. The potential environmental impact of engineered nanomaterials. *Nat. Biotechnol.* **2003**, *21* (10), 1166–1170.

(12) Petosa, A. R.; Jaisi, D. P.; Quevedo, I. R.; Elimelech, M.; Tufenkji, N. Aggregation and deposition of engineered nanomaterials in aquatic environments: Role of physicochemical interactions. *Environ. Sci. Technol.* **2010**, *44* (17), 6532–6549.

(13) Long, T. C.; Saleh, N.; Tilton, R. D.; Lowry, G. V.; Veronesi, B. Titanium dioxide (P25) produces reactive oxygen species in immortalized brain microglia (BV2): Implications for nanoparticle neurotoxicity. *Environ. Sci. Technol.* **2006**, *40* (14), 4346–4352.

(14) Kajihara, M. Settling velocity and porosity of large suspended particle. *J. Oceanogr.* **1971**, *27* (4), 158–162.

(15) Elimelech, M. *Particle Deposition and Aggregation: Measurement, Modelling, And Simulation*. Butterworth-Heinemann: Boston, 1995; p xv.

(16) Areepitak, T.; Ren, J. Model simulations of particle aggregation effect on colloid exchange between streams and streambeds. *Environ. Sci. Technol.* **2011**null-null.

(17) Sharma, V. K. Aggregation and toxicity of titanium dioxide nanoparticles in aquatic environment—A review. *J. Environ. Sci. Health, Part A: Environ. Sci. Eng.* **2009**, *44* (14), 1485–1495.

(18) Zhang, Y.; Chen, Y.; Westerhoff, P.; Hristovski, K.; Crittenden, J. C. Stability of commercial metal oxide nanoparticles in water. *Water Res.* **2008**, *42* (8−9), 2204–2212.

(19) Guzman, K. A. D.; Finnegan, M. P.; Banfield, J. F. Influence of suffface potential on aggregation and transport of titania nanoparticles. *Environ. Sci. Technol.* **2006**, *40* (24), 7688–7693.

(20) Keller, A. A.; Wang, H. T.; Zhou, D. X.; Lenihan, H. S.; Cherr, G.; Cardinale, B. J.; Miller, R.; Ji, Z. X. Stability and aggregation of metal oxide nanoparticles in natural aqueous matrices. *Environ. Sci. Technol.* **2010**, *44* (6), 1962–1967.

(21) Ji, Z.; Jin, X.; George, S.; Xia, T.; Meng, H.; Wang, X.; Suarez, E.; Zhang, H.; Hoek, E. M. V.; Godwin, H.; Nel, A. E.; Zink, J. I. Dispersion and stability optimization of TiO_2 nanoparticles in cell culture media. *Environ. Sci. Technol.* **2010**, *44* (19), 7309–7314.

(22) Jiang, J. K.; Oberdorster, G.; Biswas, P. Characterization of size, surface charge, and agglomeration state of nanoparticle dispersions for toxicological studies. *J. Nanopart. Res.* **2009**, *11* (1), 77–89.

(23) Baveye, P.; Laba, M. Aggregation and toxicology of titanium dioxide nanoparticles. *Environ. Health Perspect.* **2008**, *116* (4), A152–A152.

(24) French, R. A.; Jacobson, A. R.; Kim, B.; Isley, S. L.; Penn, R. L.; Baveye, P. C. Influence of Ionic strength, pH, and cation valence on aggregation kinetics of titanium dioxide nanoparticles. *Environ. Sci. Technol.* **2009**, *43* (5), 1354–1359.

(25) Baalousha, M. Aggregation and disaggregation of iron oxide nanoparticles: Influence of particle concentration, pH and natural organic matter. *Sci. Total Environ.* **2009**, *407* (6), 2093–2101.

(26) Thio, B. J. R.; Zhou, D. X.; Keller, A. A. Influence of natural organic matter on the aggregation and deposition of titanium dioxide nanoparticles. *J. Hazard. Mater.* **2011**, *189* (1−2), 556–563.

(27) He, Y. T.; Wan, J. M.; Tokunaga, T. Kinetic stability of hematite nanoparticles: The effect of particle sizes. *J. Nanopart. Res.* **2008**, *10* (2), 321–332.

(28) Huynh, K. A.; Chen, K. L. Aggregation kinetics of citrate and polyvinylpyrrolidone coated silver nanoparticles in monovalent and divalent electrolyte solutions. *Environ. Sci. Technol.* **2011**, *45* (13), 5564–5571.

(29) Buettner, K. M.; Rinciog, C. I.; Mylon, S. E. Aggregation kinetics of cerium oxide nanoparticles in monovalent and divalent electrolytes. *Colloids Surf., A* **2010**, *366* (1−3), 74–79.

(30) Bos, R.; van der Mei, H. C.; Busscher, H. J. Physico-chemistry of initial microbial adhesive interactions − its mechanisms and methods for study. *FEMS Microbiol. Rev.* **1999**, *23* (2), 179–230.

(31) Grasso, D.; Subramaniam, K.; Butkus, M.; Strevett, K.; Bergendahl, J. A review of non-DLVO interactions in environmental colloidal systems. *Rev. Environ. Sci. Bio/Technol.* **2002**, *1* (1), 17–38.

(32) Hermansson, M. The DLVO theory in microbial adhesion. *Colloids Surf., B* **1999**, *14* (1−4), 105–119.

(33) Hong, Y. S.; Honda, R. J.; Myung, N. V.; Walker, S. L. Transport of iron-based nanoparticles: Role of magnetic properties. *Environ. Sci. Technol.* **2009**, *43* (23), 8834–8839.

(34) Honig, E. P.; Roeberse., Gj; Wiersema, P. H. Effect of hydrodynamic interaction on coagulation rate of hydrophobic colloids. *J. Colloid Interface Sci.* **1971**, *36* (1), 97–109.

(35) Alimohammadi, M.; Fichthorn, K. A. Molecular dynamics simulation of the aggregation of titanium dioxide nanocrystals: Preferential alignment. *Nano Lett.* **2009**, *9* (12), 4198–4203.

(36) Maisels, A.; Kruis, F. E.; Fissan, H. Direct simulation Monte Carlo for simultaneous nucleation, coagulation, and surface growth in dispersed systems. *Chem. Eng. Sci.* **2004**, *59* (11), 2231–2239.

(37) Markutsya, S.; Subramaniam, S.; Vigil, R. D.; Fox, R. O. On Brownian dynamics simulation of nanoparticle aggregation. *Ind. Eng. Chem. Res.* **2008**, *47* (10), 3338–3345.

(38) Zhao, H.; Maisels, A.; Matsoukas, T.; Zheng, C. Analysis of four Monte Carlo methods for the solution of population balances in dispersed systems. *Powder Technology* **2007**, *173* (1), 38–50.

(39) Peng, Z. B.; Doroodchi, E.; Evans, G. DEM simulation of aggregation of suspended nanoparticles. *Powder Technol.* **2010**, *204* (1), 91–102.

(40) Jiang, W. T.; Ding, G. L.; Peng, H.; Hu, H. T. Modeling of nanoparticles' aggregation and sedimentation in nanofluid. *Curr. Appl. Phys.* **2010**, *10* (3), 934–941.

(41) Lin, Y. L.; Lee, K.; Matsoukas, T. Solution of the population balance equation using constant-number Monte Carlo. *Chem. Eng. Sci.* **2002**, *57* (12), 2241–2252.

(42) Smith, M.; Matsoukas, T. Constant-number Monte Carlo simulation of population balances. *Chem. Eng. Sci.* **1998**, *53* (9), 1777–1786.

(43) Lee, K.; Matsoukas, T. Simultaneous coagulation and break-up using constant-N Monte Carlo. *Powder Technol.* **2000**, *110* (1−2), 82–89.

(44) Kim, T.; Lee, C. H.; Joo, S. W.; Lee, K. Kinetics of gold nanoparticle aggregation: Experiments and modeling. *J. Colloid Interface Sci.* **2008**, *318* (2), 238–243.

(45) Kruis, F. E.; Maisels, A.; Fissan, H. Direct simulation Monte Carlo method for particle coagulation and aggregation. *AIChE J.* **2000**, *46* (9), 1735–1742.

(46) Zhao, H. B.; Zheng, C. G.; Xu, M. H. Multi-Monte Carlo method for particle coagulation: Description and validation. *Appl. Math. Comput.* **2005**, *167* (2), 1383–1399.

(47) Friedlander, S. K. *Smoke, Dust, And Haze: Fundamentals of Aerosol Dynamics*, 2nd ed.; Oxford University Press: New York, 2000; p xx.

(48) Kruyt, H. R. *Colloid Science*; Elsevier: New York, 1949.

(49) Liu, R.; Rallo, R.; George, S.; Ji, Z. X.; Nair, S.; Nel, A. E.; Cohen, Y. Classification nanoSAR development for cytotoxicity of metal oxide nanoparticles. *Small* **2011**, *7* (8), 1118–1126.

(50) Rallo, R.; France, B.; Liu, R.; Nair, S.; George, S.; Damoiseaux, R.; Giralt, F.; Nel, A.; Bradley, K.; Cohen, Y. Self-organizing map analysis of toxicity-related cell signaling pathways for metal and metal oxide nanoparticles. *Environ. Sci. Technol.* **2011**, *45* (4), 1695–1702.

(51) Allouni, Z. E.; Cimpan, M. R.; Høl, P. J.; Skodvin, T.; Gjerdet, N. R. Agglomeration and sedimentation of TiO_2 nanoparticles in cell culture medium. *Colloids Surf., B* **2009**, *68* (1), 83–87.

(52) Tiraferri, A.; Chen, K. L.; Sethi, R.; Elimelech, M. Reduced aggregation and sedimentation of zero-valent iron nanoparticles in the presence of guar gum. *J. Colloid Interface Sci.* **2008**, *324* (1−2), 71–79.

(53) Fedele, L.; Colla, L.; Bobbo, S.; Barison, S.; Agresti, F. Experimental stability analysis of different water-based nanofluids. *Nanoscale Res. Lett.* **2011**, *6* (1), 300.

(54) Li, X. F.; Zhu, D. S.; Wang, X. J. Evaluation on dispersion behavior of the aqueous copper nano-suspensions. *J. Colloid Interface Sci.* **2007**, *310* (2), 456–463.

(55) Hunter, R. J. *Foundations of Colloid Science*, 2nd ed.; Oxford University Press: New York, 2001; p xii.

(56) Filella, M.; Zhang, J. W.; Newman, M. E.; Buffle, J. Analytical applications of photon correlation spectroscopy for size distribution measurements of natural colloidal suspensions: Capabilities and limitations. *Colloids Surf., A* **1997**, *120* (1−3), 27–46.

(57) Chen, K. J.; Wolahan, S. M.; Wang, H.; Hsu, C. H.; Chang, H. W.; Durazo, A.; Hwang, L. P.; Garcia, M. A.; Jiang, Z. K.; Wu, L.; Lin, Y. Y.; Tseng, H. R. A small MRI contrast agent library of gadolinium-(III)-encapsulated supramolecular nanoparticles for improved relaxivity and sensitivity. *Biomaterials* **2011**, *32* (8), 2160–2165.

(58) Vold, R. D.; Vold, M. J. *Colloid and Interface Chemistry*; Addison-Wesley: Reading, MA, 1983; p xxv.

(59) Schwarzer, H. C.; Peukert, W. Prediction of aggregation kinetics based on surface properties of nanoparticles. *Chem. Eng. Sci.* **2005**, *60* (1), 11–25.

(60) Brant, J.; Lecoanet, H.; Wiesner, M. R. Aggregation and deposition characteristics of fullerene nanoparticles in aqueous systems. *J. Nanopart. Res.* **2005**, *7* (4−5), 545–553.

(61) Chen, K. L.; Elimelech, M. Relating colloidal stability of fullerene (C_{60}) nanoparticles to nanoparticle charge and electrokinetic properties. *Environ. Sci. Technol.* **2009**, *43* (19), 7270–7276.

(62) Gomez-Merino, A. L.; Rubio-Hernandez, F. J.; Velazquez-Navarro, J. F.; Galindo-Rosales, F. J.; Fortes-Quesada, P. The Hamaker

constant of anatase aqueous suspensions. *J. Colloid Interface Sci.* **2007**, *316* (2), 451–456.

(63) Visser, J. On Hamaker constants: A comparison between Hamaker constants and Lifshitz-van der Waals constants. *Adv. Colloid Interface Sci.* **1972**, *3* (4), 331–363.

(64) Ackler, H. D.; French, R. H.; Chiang, Y. M. Comparisons of Hamaker constants for ceramic systems with intervening vacuum or water: From force laws and physical properties. *J. Colloid Interface Sci.* **1996**, *179* (2), 460–469.